Appl. Phys. A 79, 125–129 (2004)
DOI: 10.1007/s00339-003-2329-8

Applied Physics A
Materials Science & Processing

J.E. ATWATER✉
R.R. WHEELER, JR.

Microwave permittivity and dielectric relaxation of a high surface area activated carbon

UMPQUA Research Company, P.O. Box 609, Myrtle Creek, Oregon 97457, USA

Received: 12 March 2003/Accepted: 30 July 2003
Published online: 1 October 2003 •

ABSTRACT Carbonaceous materials are amenable to microwave heating to varying degrees. The primary indicator of susceptibility is the complex permittivity (ε^*), of which, the real component correlates with polarization, and the imaginary term represents dielectric loss. For a given material, the complex permittivity is dependent upon both frequency and temperature. Here we report the complex permittivity of a high surface area coconut shell activated carbon which is commonly used in analytical chemistry and a wide variety of industrial separations. Associated polarization-relaxation phenomena are also characterized. Broadband measurements were made using a high temperature compatible open-ended coaxial dielectric probe at frequencies between 0.2 and 26 GHz, and across the temperature region between 24 °C and 191 °C.

PACS 77.22.-d

Many granular activated carbons are highly susceptible to microwave (dielectric) heating. This may be used to advantage in the thermal treatment of activated carbons and in the thermal regeneration of loaded activated carbon based sorbents via high frequency irradiation [1]. However, much variability is evident between different forms of activated carbon [2]. Barnebey-Sutcliffe 580-26 activated carbon is an excellent quality high surface area material prepared from coconut shell charcoal and activated by treatment with high temperature steam. The material is specified for use as an adsorbent in the determination of volatile organic contaminants by purge and trap gas chromatography using U.S. Environmental Protection Agency (EPA) Methods 502.1, 502.2, 524.1, 524.2, 601, and 8240. Researchers in our laboratory have employed this type of activated carbon as an adsorbent for liquid phase organic contaminants in water purification systems designed for the International Space Station [3], and also in microwave powered thermally regenerable systems for the removal of airborne organic contaminants [1, 4]. To quantitate the susceptibility of this material to dielectric heating as a function of frequency and temperature, complex permittivities were determined at microwave frequencies between 0.2–26 GHz, and over the temperature range between 24 °C–191 °C using an open-ended coaxial dielectric probe [5–8]. Though less accurate than fixed frequency waveguide and resonator based methods, the coaxial probe technique provides the capability for determination of dielectric properties over a wide frequency range.

In non-magnetic media, susceptibility to microwave heating is governed by the frequency (ω) dependent complex permittivity [9, 10],

$$\varepsilon^*(\omega) = \varepsilon'(\omega) - \mathrm{i}\varepsilon''(\omega)\,. \tag{1}$$

The terms of ε^* are described by the Kramers–Kronig relations

$$\varepsilon'(\omega) = \varepsilon_\infty + \frac{2}{\pi}\int_0^\infty \frac{\varepsilon''(\omega)\omega'}{(\omega')^2 - \omega^2}\,\mathrm{d}\omega'\,, \tag{2}$$

$$\varepsilon''(\omega) = \frac{2}{\pi}\int_0^\infty \frac{[\varepsilon'(\omega) - \varepsilon_\infty]\omega}{(\omega')^2 - \omega^2}\,\mathrm{d}\omega'\,, \tag{3}$$

where ε_∞ is permittivity at the high frequency limit, and ω' is an integration variable [11]. In the complex plane, the real and imaginary terms of $\varepsilon^*(\omega)$ correlate with polarization, and energy loss, respectively. The dielectric loss factor or dissipation factor ($\tan\delta$) is defined as,

$$\tan\delta = \frac{\omega\varepsilon''(\omega)\,|\boldsymbol{E}_\mathrm{o}|^2}{\omega\varepsilon'(\omega)\,|\boldsymbol{E}_\mathrm{o}|^2} = \frac{\varepsilon''(\omega)}{\varepsilon'(\omega)}\,. \tag{4}$$

This represents the fractional power loss as compared to power stored. The average power per unit volume (P) consumed by loss mechanisms can then be calculated as,

$$P = \frac{1}{2}\omega\varepsilon''\,|\boldsymbol{E}_\mathrm{o}|^2 \tag{5}$$

The attenuation of a microwave beam directed along the x-axis by an absorbing material is described by [12],

$$P(x) = P_\mathrm{o}\exp(-2\alpha x) \tag{6}$$

where the attenuation coefficient (α) is a function of the angular frequency (ω), complex permittivity, and complex permea-

✉ Fax: +1-541/863-7775, E-mail: jatwater@urcmail.net

bility (μ^*),

$$\alpha = \omega\sqrt{\sqrt{\varepsilon'^2+\varepsilon''^2}\sqrt{\mu'^2+\mu''^2}} \times \sin\left[\frac{\arctan\left(\frac{\varepsilon''}{\varepsilon'}\right)+\arctan\left(\frac{\mu''}{\mu'}\right)}{2}\right]. \quad (7)$$

In non-magnetic materials, values of μ^* are extremely low, hence, microwave absorption is dominated by the complex permittivity terms. From this, it is clear that knowledge of the frequency and temperature dependencies of complex permittivity in the microwave region of the electromagnetic spectrum for a given granular activated carbon may be quite useful in the modeling and design of dielectric heating systems.

1 Experimental

The apparatus used to acquire complex permittivity data is illustrated schematically in Fig. 1. The integrated system consists of a Vector Network Analyzer (VNA) and a high temperature compatible open-ended coaxial dielectric probe [13–15]. While the VNA was capable of operation between 0.05–40 GHz, limitations of the dielectric probe and associated transmission elements reduced the practical working frequency range to between 0.2 and 26 GHz. Using this method dissipation ($\tan\delta$) factors ≥ 0.05 are required to assure accuracy of the test results. Complex permittivity measurements were made under software control via a Hewlett-Packard Interface Bus (HPIB) parallel connection between the computer and the VNA. In operation, the VNA scans a preset frequency range over which transmission and reflection parameters are determined. Material in direct contact with the coaxial dielectric probe alters the phases and magnitudes of reflected power observed by the VNA. Complex permittivities were calculated using the methods described by Blackham and Pollard [16].

To measure complex permittivities at elevated temperatures, the dielectric probe was mounted inside a gravity convection oven. To minimize temperature gradients, the oven was modified by sealing the external air convection current ports, and the addition of an internal recirculation fan. Improved temperature control was achieved using a digital PID controller and a K-type thermocouple probe mounted inside the oven. A 610 mm precision mercury thermometer covering the temperature range between −1 °C to 201 °C with 0.2 °C resolution was used to monitor the temperature of the test specimen. Both the thermocouple probe and the mercury thermometer were inserted into a sand-filled beaker of equivalent volume and elevation within the oven as the material under study. A high temperature semi-rigid coaxial cable was used to connect the oven mounted dielectric probe with the external VNA. Access for the thermocouple, thermometer, and coaxial cable was established through a 5.0 cm diameter insulation filled circular opening at the top of the oven. Temperature regulation was accurate to within 0.2 °C. Experiments conducted to confirm the validity of data obtained using this system have been described previously [17, 18].

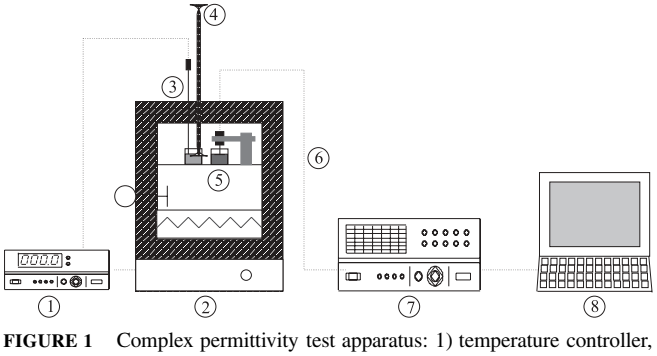

FIGURE 1 Complex permittivity test apparatus: 1) temperature controller, 2) oven, 3) thermocouple, 4) Hg thermometer, 5) coaxial dielectric probe immersed in sample, 6) high temperature semi-rigid coaxial cable, 7) vector network analyzer, and 8) computer

BET surface area of Barnebey-Sutcliffe 580-26 activated carbon (Columbus, Ohio), with particle sizes ranging between 710 μm and 1500 μm, was determined by nitrogen adsorption porosimetry using a Micromeritics Gemini model surface area analyzer [19]. High resolution images of the carbon surface were obtained using a JEOL model JSM6300 XV Scanning Electron Microscope (SEM). Permittivity measurements were performed at five temperatures covering the approximate range between 20–200 °C. Samples were presented to the instrument as fine powders, thus obviating the need to correct for the effects of intergranular porosity [20–24]. To minimize interference from adsorbed water, samples were dried at 180 °C for a minimum of 72 hours, and then stored in a dessicator prior to analysis. The instrument was first calibrated, followed by duplicate measurements at ambient temperature, with the coaxial dielectric probe in intimate contact with the material under study. The temperature was then increased. Once the set-point temperature was reached, a period of 45 minutes was allowed for the system to stabilize. Then a second set of duplicate measurements were made. This procedure was followed until data covering the full temperature span were gathered. The numerical values of all complex permittivities were calculated as dimensionless relative permittivities ($\varepsilon^*/\varepsilon_o$). These may be converted to absolute permittivities through multiplication by the permittivity of free space (ε_o), in appropriate units.

2 Results and discussion

The microporous nature of this activated carbon is clear from the SEM photomicrographs presented in Fig. 2. A high degree of heterogeneity is also evident. This microporosity correlates with the measured BET surface area of 1756 m^2/g. Surface affinity characteristics, porosity and the extremely high surface area of this activated carbon are the primary factors which account for its excellence as an adsorbent for both gas-phase and aqueous organic contaminants. As indicated in Figs. 3 and 4, this activated carbon interacts very strongly with an incident microwave beam. At each temperature, the real component of the complex permittivity (Fig. 3) decreases smoothly with increasing frequency. Maxima are evident at the low frequency limit (0.2 GHz), with ε' values increasing with temperature from 97 at 24.1 °C to 159.4 at 191 °C. At frequencies greater than 10 GHz, ε' values for all temperatures converge, yielding minimum values of ∼ 10 at the high frequency limit (26 GHz). Dielectric loss fac-

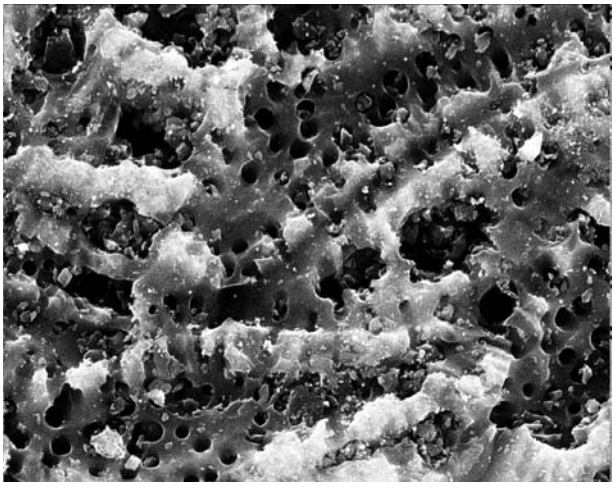

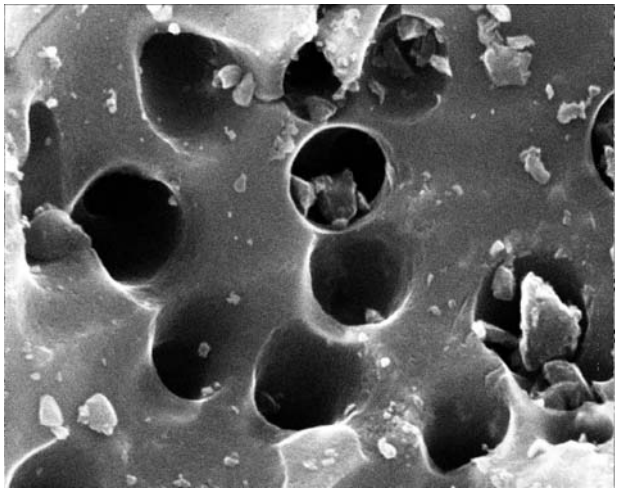

FIGURE 2 Scanning electron micrographs of Barnebey–Sutcliffe 580-26 activated carbon. *Top* X2,000, *Bottom* X 10,000 magnification

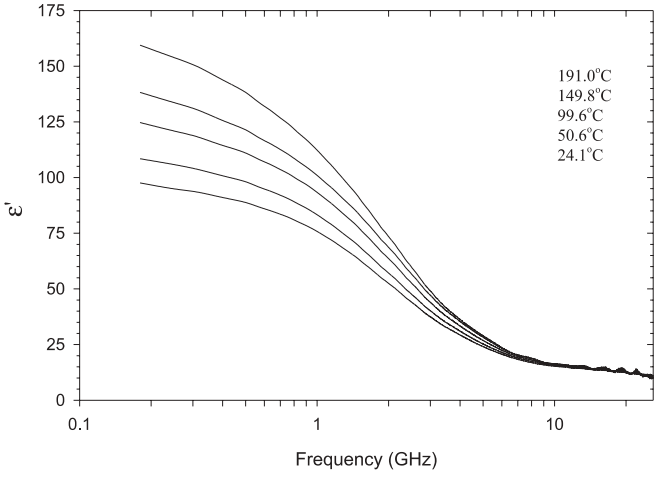

FIGURE 3 Real component of complex permittivity vs. frequency and temperature

tors (ε'') increase with frequency to maximum values near 2 GHz and then decrease to minimum values at the high frequency limit (Fig. 4). For all but the very highest frequency region, dielectric loss is strongly temperature dependent. The approximately linear relationships between temperature and ε'' for a range of frequencies is illustrated in Fig. 5. Maximum values for dielectric loss range from 40.8 at 24.1 °C to 70.5 at 191 °C, corresponding to tan δ (dissipation factor) values which increase smoothly from 0.777 to 0.836 over this temperature range. The strongest temperature effects on ε'' are evident between 149.8 °C and 191 °C in the frequency range between 0.2–2 GHz. This is an important phenomenon to consider for practical microwave heating applications, as care must be taken to prevent thermal runaway.

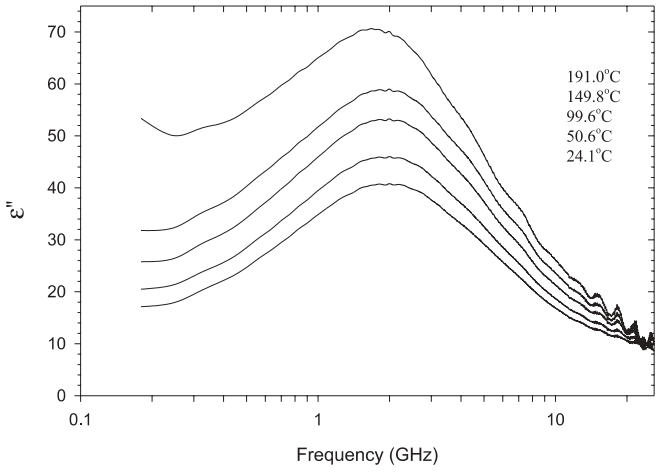

FIGURE 4 Imaginary component of complex permittivity vs. frequency and temperature

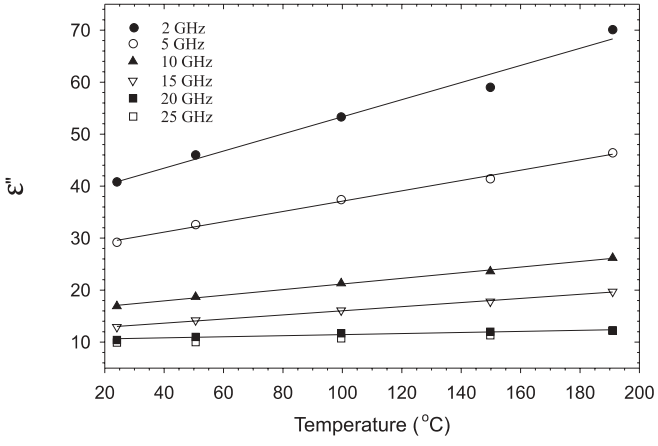

FIGURE 5 Dielectric loss versus temperature for a range of microwave frequencies

From these data, dielectric relaxation phenomena are clearly evident. In susceptible solids, heat is produced via oscillating induced interfacial (Maxwell–Wagner) and space-charge polarizations [25–31]. Polarization-relaxation phenomena have been described by Debye as

$$\varepsilon^*(\omega) = \varepsilon_\infty + \frac{\varepsilon_s - \varepsilon_\infty}{1 + i\omega\tau} \tag{8}$$

where ε_s is the static (zero frequency) permittivity and τ represents the polarization relaxation time, which is the inverse of the frequency of maximum dielectric loss [25]. The real and imaginary components of the complex permittivity are then

described as

$$\varepsilon'(\omega) = \varepsilon_\infty + \frac{\varepsilon_s - \varepsilon_\infty}{1 + (\omega\tau)^2}\,, \tag{9}$$

$$\varepsilon''(\omega) = \frac{\varepsilon_s - \varepsilon_\infty}{1 + (\omega\tau)^2}\omega\tau\,. \tag{10}$$

In the slightly more complex Cole–Cole model [26] the $i\omega\tau$ term is raised to the power of β. Here, the individual permittivity terms [27] can be described as,

$$\varepsilon'(\omega) = \varepsilon_\infty + \frac{(\varepsilon_s - \varepsilon_\infty)}{2}\left[1 - \frac{\sinh(\beta \ln \omega\tau)}{\cosh(\beta \ln \omega\tau) + \cos\left(\frac{\beta\pi}{2}\right)}\right], \tag{11}$$

$$\varepsilon''(\omega) = \frac{(\varepsilon_s - \varepsilon_\infty)\sin\left(\frac{\beta\pi}{2}\right)}{2\left[\cosh(\beta \ln \omega\tau) + \cos\left(\frac{\beta\pi}{2}\right)\right]}\,. \tag{12}$$

From these relations, it follows that a plot of ε'' versus ε' in the complex plane, termed a Cole–Cole plot, will form a semicircle centered at,

$$\varepsilon'(\omega) = \frac{\varepsilon_s + \varepsilon_\infty}{2}\,, \tag{13}$$

in which β is the central angle of circular arc for the dielectric loss. A Cole–Cole plot for the coconut shell activated carbon is shown in Fig. 6. In this representation, data are presented as symbols and the fit established using (11) and (12) are shown as dashed lines. The derived polarization-relaxation parameters, including the relaxation time constants and values of β, are summarized in Table 1. These data are anamolous in that the relaxation time increases with temperature, as illustrated in Fig. 7.

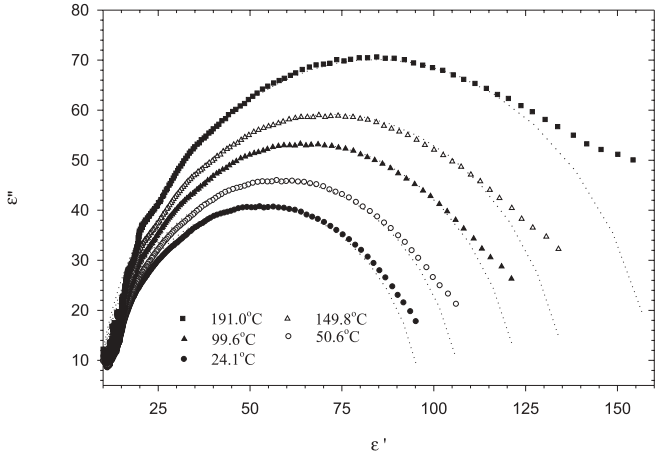

FIGURE 6 Cole–Cole plot for coconut shell activated carbon

T °C	τ 10^{-11} s	β	ε_{rs} [a]	ε_∞ [b]
24.1	7.73	0.945	97.0	8.0
50.6	8.25	0.945	108	8.0
99.6	8.51	0.945	124	8.0
149.8	8.56	0.945	137	8.0
191.0	9.53	0.945	161	8.0

a ε_{rs} is the relative static dielectric permittivity ($\varepsilon_s/\varepsilon_o$)
b ε_∞ is the relative dielectric permittivity at the high frequency limit ($\varepsilon_\infty/\varepsilon_o$)

TABLE 1 Summary of Cole–Cole polarization-relaxation parameters

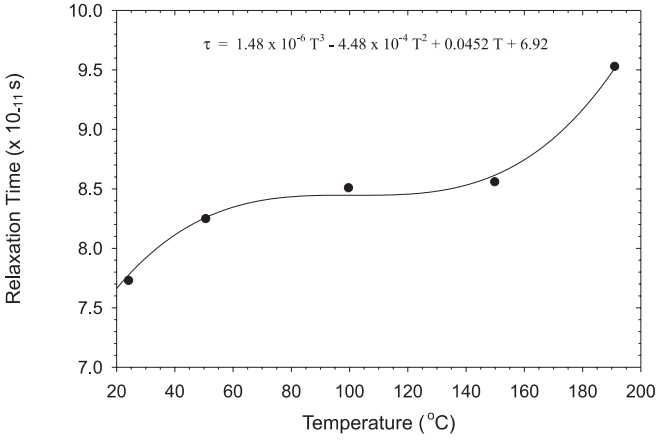

FIGURE 7 Polarization relaxation time versus temperature

3 Conclusions

This high quality coconut shell activated carbon couples effectively with microwaves across the full energy spectrum, and hence, is highly susceptible to microwave dielectric heating. For all temperatures investigated, the dissipation factor ($\tan\delta$) rises with increasing frequency to maxima near 7 GHz. Both the dissipation factor and the dielectric loss factor increase significantly with temperature; hence, in practical heating applications for this material, care must be taken to preclude thermal run-away. The polarization-relaxation equations accurately describe the experimental results over the frequency range between 800 MHz and 26 GHz. The deviation from semicircular symmetry in the Cole–Cole plot (Fig. 6) at lower frequencies (right hand region) is most likely due to the effects of electrical conductivity of the medium. The observed temperature dependence of the polarization relaxation time for this high surface area activated carbon does not follow that of conventional solids. This relationship can be described by the Erying formalism,

$$\tau(T) = \frac{h}{kT}\exp\left(\frac{\Delta H}{RT}\right)\exp\left(-\frac{\Delta S}{R}\right)\,, \tag{14}$$

where h, and k are Planck and Boltzmann constants, and H and S represent enthalpy and entropy of activation, respectively [32]. Above ~ 100 K, the temperature dependence of the pre-exponential factor becomes relatively insignificant, and the relationship simplifies to the Arrhenius equation,

$$\tau(T) = \tau_0 \exp\left(\frac{E_a}{RT}\right)\,, \tag{15}$$

where,

$$\tau_0 = \frac{h}{kT}\exp\left(-\frac{\Delta S}{R}\right)\,. \tag{16}$$

These expressions describe relaxation times which decrease exponentially with absolute temperature. However, polarization relaxation times for the Barnebey–Sutcliffe 580-26 activated carbon increase with temperature. Though unusual, deviation from normal temperature versus polarization-relaxation time trends has been observed in another form of activated carbon [2]. The anomalous behavior may in some way be an artifact of the extreme heterogeneity of the material, or may be the result of chemical or structural changes which occur as the temperature is increased, and which affect polarization within the material.

ACKNOWLEDGEMENTS This work was funded by the Ames Research Center of the National Aeronautics and Space Administration under contract NAS2-97017. The authors are grateful to Dr. Bernadette K. Luna for her support of this project.

REFERENCES

1 J.E. Atwater, J.T. Holtsnider, R.R. Wheeler, Jr.: *Microwave regenerable air purification device* (National Technical Information Service, Springfield, Virginia 1996)
2 J.E. Atwater, R.R. Wheeler, Jr.: Carbon **41**, 1801 (2003)
3 D.F. Putnam, W.F. Michalek, T. Van Pelt: in *Spacecraft water quality: maintenance and monitoring*, ed. by R.L. Sauer, R.M. Bagdigian (SAE, Warrendale, Pennsylvania 1991) pp. 189–194
4 R.R. Wheeler, Jr., J.E. Atwater, J.R. Akse, J.T. Holtsnider, B. Luna: SAE Technical Paper No. 2002-01-2403 (2002)
5 G. Gajda, S.S. Stuchly: IEEE Trans. Instrum. Meas. **30**, 506 (1981)
6 M.A. Stuchly, M.M. Brady, S.S. Stuchly, G. Gajda: IEEE Trans. Instrum. Meas. **31**, 116 (1982)
7 T.P. Marsland, S. Evans: Proc. IEE, **134** H, 341 (1987).
8 D. Misra, M. Chabbra, B.R. Epstein, M. Mirotznik, K.R. Foster: IEEE Trans. Microwave Theory Tech. **38**, 8 (1990)
9 A. von Hippel: *Dielectrics and Waves* (Wiley, New York 1954)
10 A. von Hippel (Ed.): *Dielectric Materials and Applications* (Technology Press of MIT, Cambridge 1954)
11 A.K. Jonscher: *Dielectric Relaxation in Solids* (Chelsea Dielectrics Press, London 1983)
12 A.C. Mataxas, R.J. Meridith: *Industrial Microwave Heating* (Peter Perigrinus, Ltd., London 1983)
13 B. Colpitts: IEEE Trans. Microwave Theory Tech. **41**, 229 (1993)
14 S. Bringhurst, M.F. Iskander: IEEE Trans. Microwave Theory Tech. **44**, 926 (1996)
15 D.L. Gershon, J.P. Calame, Y. Carmel, T.M. Antonsen, Jr., R.M. Hutcheon: IEEE Trans. Microwave Theory Tech. **47**, 1640 (1999)
16 D.V. Blackham, R.D. Pollard: IEEE Trans. Instrum. Meas. **46**, 1093 (1997)
17 J.E. Atwater: Carbohydr. Res. **327**, 219 (2000)
18 J.E. Atwater: Appl. Phys. A **75**, 555 (2002)
19 S. Brunauer, P.H. Emmett, E. Teller: J. Am. Chem. Soc. **60**, 309 (1938)
20 B. Nost, B.D. Hansen, E. Haslund: Physica Scripta **T44**, 67 (1992)
21 D. Polder, J.H. van Santen: Physica **12**, 257 (1946)
22 A. Stogryn: IEEE Trans. Antennas Propagat. **AP-32**, 517 (1984)
23 L.S. Taylor: IEEE Trans. Antennas Propagat. **AP-13**, 943 (1965)
24 L. Tsang, J.A. Kong: Radio Sci. **16**, 303 (1981)
25 P. Debye: *Polar Molecules* (Lancaster Press, Lancaster, Pennsylvania 1929)
26 K.S. Cole, R.H. Cole: J. Chem. Phys. **9**, 341 (1941)
27 T. Ohgushi, K. Isimaru: Phys. Chem. Chem. Phys. **3**, 3229 (2001)
28 C.J.F. Bottcher: *Theory of Electric Polarization* (Elsevier, New York 1952)
29 S. Havriliak, Jr., S.J. Havriliak: *Dielectric and Mechanical Relaxation in Materials* (Hanser, New York 1997)
30 V.I. Gaiduk: *Dielectric Relaxation and Dynamics of Polar Molecules* (World Scientific, New Jersey 1999)
31 A.K. Jonscher: J. Phys. D: Appl. Phys. **32**, R57 (1999)
32 N.T. Correia, J.J.M. Ramos: Phys. Chem. Chem. Phys. **2**, 5712 (2000)